Biophysical Journal
Article

Biophysical Society

Friction from Transduction Channels' Gating Affects Spontaneous Hair-Bundle Oscillations

Jérémie Barral,[1,2] Frank Jülicher,[3,4] and Pascal Martin[1,2,4,*]
[1]Laboratoire Physico-Chimie Curie, Institut Curie, PSL Research University, CNRS, UMR168, Paris, France; [2]UPMC Université Paris 06, Sorbonne Universités, Paris, France; [3]Max Planck Institute for the Physics of Complex Systems, Dresden, Germany; and [4]Kavli Institute for Theoretical Physics, University of California-Santa Barbara, Santa Barbara, California

ABSTRACT Hair cells of the inner ear can power spontaneous oscillations of their mechanosensory hair bundle, resulting in amplification of weak inputs near the characteristic frequency of oscillation. Recently, dynamic force measurements have revealed that delayed gating of the mechanosensitive ion channels responsible for mechanoelectrical transduction produces a friction force on the hair bundle. The significance of this intrinsic source of dissipation for the dynamical process underlying active hair-bundle motility has remained elusive. The aim of this work is to determine the role of friction in spontaneous hair-bundle oscillations. To this end, we characterized key oscillation properties over a large ensemble of individual hair cells and measured how viscosity of the endolymph that bathes the hair bundles affects these properties. We found that hair-bundle movements were too slow to be impeded by viscous drag only. Moreover, the oscillation frequency was only marginally affected by increasing endolymph viscosity by up to 30-fold. Stochastic simulations could capture the observed behaviors by adding a contribution to friction that was 3–8-fold larger than viscous drag. The extra friction could be attributed to delayed changes in tip-link tension as the result of the finite activation kinetics of the transduction channels. We exploited our analysis of hair-bundle dynamics to infer the channel activation time, which was ∼1 ms. This timescale was two orders-of-magnitude shorter than the oscillation period. However, because the channel activation time was significantly longer than the timescale of mechanical relaxation of the hair bundle, channel kinetics affected hair-bundle dynamics. Our results suggest that friction from channel gating affects the waveform of oscillation and that the channel activation time can tune the characteristic frequency of the hair cell. We conclude that the kinetics of transduction channels' gating plays a fundamental role in the dynamic process that shapes spontaneous hair-bundle oscillations.

INTRODUCTION

The cellular microphones of the inner ear—the hair cells—are each endowed with a hair bundle that extends from the cell's apical surface into the surrounding fluid. The hair bundle works as a mechanosensory antenna: sound evokes periodic deflections of the hair bundle, which elicits a receptor current through the hair cell by gating mechanosensitive transduction channels (1). Remarkably, the hair cell can power spontaneous oscillations of its hair bundle, resulting in frequency-selective amplification of weak inputs near the characteristic frequency of spontaneous oscillation (2–5).

Understanding the physical parameters that control the oscillation properties is of crucial importance to clarify how these properties may be tuned to provide sensitive detection at different frequencies (6,7). We focus here on friction, which by providing a source of mechanical noise and by impeding hair-bundle vibrations, challenges the sensitivity and limits the deflection velocity of a hair bundle (8–10). Recently, dynamic force measurements on oscillatory hair bundles from the bullfrog's sacculus have revealed that gating of the transduction channels is associated with an effective friction force on the micron-sized hair bundle, hereafter called "gating friction" (9).

Gating friction is intimately related to the physics of hair-cell mechanosensitivity. Mechanosensitivity stems from direct activation of ion channels by tension changes in the tip links of the hair bundle (11). As transduction channels open or close, the extension of the tip links or of more compliant elements in series with the tip links decreases or increases, respectively, resulting in a change in tip-link tension (12). Thus, gating of transduction channels produces a force on the hair bundle. Gating forces affect

Submitted June 21, 2017, and accepted for publication November 14, 2017.
*Correspondence: pascal.martin@curie.fr
Jérémie Barral's present address is Center for Neural Science, New York University, New York.
Editor: Jennifer Curtis.
https://doi.org/10.1016/j.bpj.2017.11.019

the mechanical properties of the whole hair bundle. First, they effectively reduce the stiffness of the hair bundle, a phenomenon called "gating compliance" (13). Gating compliance can be strong enough to yield negative stiffness, providing a mechanical instability that is necessary for the emergence of spontaneous oscillations (14). Second, gating forces also effectively increase friction on the hair bundle. This is because the finite activation kinetics of the transduction channels delays changes of tip-link tension evoked by channel gating (9,15). As the hair bundle moves back and forth, delayed changes in tip-link tension result in hysteresis and energy dissipation. Interestingly, it was found that gating friction can dominate viscous drag by endolymph on the hair bundle. This finding raises the possibility that gating friction may play an important role in the dynamic process that shapes spontaneous hair-bundle oscillations and sets their characteristic frequency.

Here, we studied the statistical properties of hair-bundle movements over a large ensemble of hair cells and for different viscosities of the fluid that bathes the hair bundle. Combining experiments with theory, we identified signatures of gating friction on hair-bundle dynamics. Although the channel activation time is two orders of magnitude lower than the oscillation period, we found that channel kinetics provides a key determinant of the oscillation waveform and frequency.

MATERIALS AND METHODS

Experimental preparation

All experimental procedures were performed in accordance with European and the French National Regulation for the Protection of Vertebrate Animals used for Experimental and other Scientific Purposes (Directive 2010/63; French Decree 2013-118). Details of the experimental procedure have been published elsewhere (16). In short, an excised preparation of the bullfrog's (*Rana catesbeiana*) sacculus was mounted on a two-compartment chamber. The basal bodies of hair cells bathed in a standard saline containing 110 mM NaCl, 2 mM KCl, 4 mM $CaCl_2$, 3 mM D-glucose, 2 mM Na_2-creatine phosphate, 2 mM Na-pyruvate, and 5 mM Na-HEPES. Hair bundles were instead immersed in an artificial endolymph composed of 2 mM NaCl, 118 mM KCl, 0.25 mM $CaCl_2$, 3 mM D-glucose and 5 mM Na-HEPES. To loosen the connection between the hair bundles and the overlying otolithic membrane, the apical surface of the preparation was exposed for 20 min to endolymph supplemented with 67 $mg \cdot mL^{-1}$ of the protease subtilisin (type XXIV; Sigma-Aldrich, St. Louis, MI). The otolithic membrane was then gently removed with an eyelash. Under such conditions, the hair bundles routinely displayed spontaneous oscillations.

Microscopic apparatus and mechanical stimulation

The preparation was viewed through a ×60 water-immersion objective of an upright microscope (BX51WI; Olympus, Shinjuku, Tokyo, Japan). Spontaneous hair-bundle oscillations were recorded by imaging, at a magnification of ×1000, the top of the longest stereociliary row onto a displacement monitor that included a dual photodiode. The contrast between the hair bundle and the surrounding endolymph was always sufficient to record oscillations of freely moving hair bundles. Calibration was performed before each recording of an oscillation by measuring the output voltages of this photometric system in response to a series of offset displacements. Before filtering, sampling, and acquisition, the signal produced by our displacement monitor went through a voltage amplifier (AMP502; Tektronics, Rocky Point, NY); the amplificatory gain was adjusted to ensure a calibration constant of ~10 mV/nm.

To characterize the mechanical properties of individual oscillatory hair bundles, the tip of a flexible glass fiber was affixed to the kinociliary bulb of the hair bundle and imaged onto the photodiodes. Stimulus fibers were pulled from borosilicate capillaries and coated with a thin layer of gold-palladium to enhance contrast. For a free fiber immersed in water, the power spectral density of fluctuations at the fiber's tip was fitted by a Lorentzian, which provided a stiffness $k_F = 100–380\ \mu N \cdot m^{-1}$ and a drag coefficient $\lambda_F = 20–100\ nN \cdot s \cdot m^{-1}$ (9). The fiber was secured by its base to a stack-type piezoelectric actuator (PA-4/12; Piezosystem Jena, Jena, Germany) driven by a custom-made power supply (Elbatech Technologies, Ashdod, Israel). Movements Δ of the fiber's base resulted in the application of a force F onto an attached hair bundle and thus in a bundle movement X.

Characterization of the force-displacement relation

Using displacement-clamp circuitry (17), we imposed step displacements to the hair bundle and measured tip and base positions of the fiber at a time 5–7 ms after the step onset. This delay ensured that the transduction channels had reached thermal equilibrium and that frictional forces had vanished. During the time window of the recording, the fiber was nearly stationary and thus subjected to no or very weak frictional forces. The applied force $F = k_F(\Delta - X)$ was purely elastic and could thus be calculated by multiplying the deflection of the fiber by the fiber's stiffness. In turn, this procedure allowed for the characterization of a bundle's elastic properties. In accordance with the gating-spring model of mechano-electrical transduction (12), we fitted the measured force-displacement relation with the equation

$$F(X) = K_\infty X - NZ\,P_o(X) + F_0, \qquad (1)$$

in which K_∞ represents the hair-bundle stiffness at large positive or negative displacements, N is the number of transduction elements operating in parallel in the hair bundle, Z is the single-channel gating force, and the constant force F_0 is such that $F(0) = 0$. The channels' open probability obeys its equilibrium expression $P_o(X) = P_\infty(X)$ with

$$P_\infty(X) = 1/[1 + \exp(-Z\,(X - X_0)/(k_B T))], \qquad (2)$$

in which X_0 is the bundle deflection at which the open probability is 1/2 and $k_B T$ represents the thermal energy, with k_B indicating the Boltzmann constant and T the temperature. The force-displacement relation of oscillatory hair bundles showed a region of negative stiffness (14).

Signal generation and acquisition

All signals were generated and acquired under the control of a computer running a user interface programmed with the software LabVIEW (version 8.6; National Instruments, Austin, TX). The command signal controlling the movement of the base of a stimulus fiber was produced by a 16-bit interface card at a sampling rate of 2.5 kHz (PCI-6733; National Instruments). A second interface card (PCI-6250; National Instruments) conducted signal acquisition with a precision of 16 bits and a sampling rate of 2.5 kHz. Signals coming from the displacement monitor or going to the stimulation apparatus were conditioned with an eight-pole Bessel antialiasing filter adjusted to a low-pass half-power frequency of 1 kHz. By recording 14 hair-bundle oscillations at a sampling rate at 15 kHz or more, we could

test whether low-pass filtering resulted in a significant reduction of the maximal speed of hair-bundle movement that was recorded (Fig. 1 *D*). We found that the effect was relatively small, for the maximal bundle speed decreased by only 1.9–7.3% (mean: 4.2%) when the cutoff frequency varied from 5 to 1 kHz.

Analysis of spontaneous oscillations

We recorded from 196 oscillatory hair bundles in 93 ears. To characterize the properties of spontaneous oscillations, we monitored the time course $X(t)$ of hair-bundle position for 30 s. The relation between the power spectral density $\tilde{C}(f)$ of the movement and frequency f peaked at a characteristic frequency f_0. We smoothed the relation $\tilde{C}(f)$ by performing a moving average over a number of points (range: 3–100) corresponding to a frequency window (0.1–4 Hz) of about one twentieth of the oscillation's frequency (2–80 Hz). We then fitted the result by the sum of two Lorentzian functions (Fig. 1 *C*); (18,19):

$$\tilde{C}(f) = \frac{A}{(f_0/2Q)^2 + (f - f_0)^2} + \frac{A}{(f_0/2Q)^2 + (f + f_0)^2}. \quad (3)$$

The fit provided numerical values for the quality factor Q, the characteristic frequency f_0, and parameter A, which is related to the root-mean-square magnitude $X_{\mathrm{RMS}} = \langle (X(t) - \langle X \rangle)^2 \rangle = \int_{-\infty}^{+\infty} \tilde{C}(f) df = \sqrt{4\pi A Q / f_0}$ of the movement.

In this study, the probability density of position of an oscillatory hair bundle was most often bimodal, although additional peaks could be observed in ~30% of oscillatory hair bundles (91 out of 287 cells), as reported before (20). Such oscillations were excluded from the analysis. We fitted bimodal position distributions by the sum of two Gaussian functions (Fig. 1 *B*) and estimated, from the fit, the fractional area under the Gaussian that was centered at a positive position with respect to the mean bundle position. As indicated by numerical simulations (Fig. S1), this quantity provided a functional estimate of the open probability $P_{o,S}$ of transduction channels at steady state, which defines the operating point of transduction apparatus. In particular, an open probability of 1/2 yielded a symmetric rectangular oscillation with equal dwell times at nearly stationary positions before position switches in the positive and the negative directions, corresponding to channel opening and closure, respectively. Indeed, direct coupling between a bundle's position and the open probability of the mechanosensitive transduction channels imposes a close correspondence between position and transduction-current waveforms of oscillation (16,17,21).

We developed an algorithm to study the kinetics of position switches during a spontaneous oscillation. The hair-bundle movement was smoothed by a moving average over a 2-ms time window. The time derivative of the resulting signal was then smoothed over the same time window. Peaks exceeding twice the SD of the smoothed derivative were defined as switches and the switch times were recorded (Fig. 1 *A*). Using the raw oscillation, positive and negative switches, respectively, were then aligned and averaged (Fig. 1 *D*). To determine the mean speed of a switch, the time derivative of the switch-triggered average, which was bell shaped (Fig. 1 *D*), was fitted by a Gaussian function. The mean speeds of positive and negative switches were not significantly different and their values were thus averaged to define the switch velocity V_{MAX}. In the following, we refer to "oscillatory properties" of a given hair bundle as a set of five parameters: $P_{o,S}$, f_0, Q, X_{RMS}, and V_{MAX}. Data analysis was performed using the software MATLAB (version R2015a; The MathWorks, Natick, MA).

Increasing viscous drag on a hair bundle

Adding a polymer of sucrose (Dextran 500, Dextran 40, or Ficoll PM 400; Amersham Biosciences, Little Chalfont, UK) into endolymph afforded a

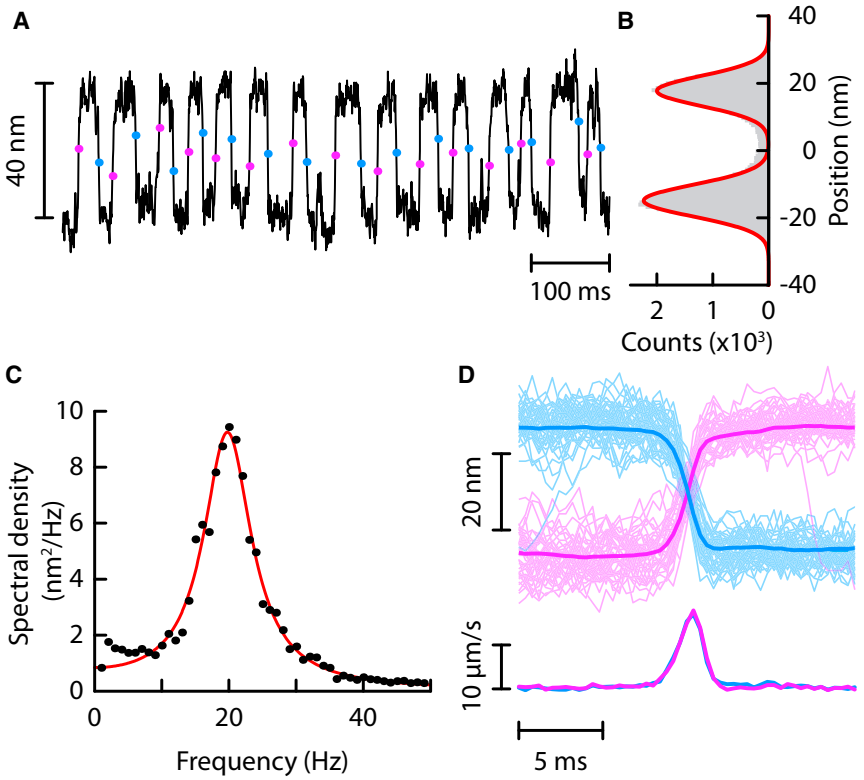

FIGURE 1 Spontaneous oscillation of the hair-cell bundle. (*A*) The time course of hair-bundle position is shown here over 15 cycles of oscillation. The bundle switched between two nearly stationary positions; the times of positive and negative switches are marked by magenta and blue disks, respectively. (*B*) The position histogram was well described by the sum of two Gaussian distributions (*red line*). The fractional area under the positive peak provided a functional estimate of the open probability of the transduction channels at steady state, here $P_{o,S} = 0.47$. (*C*) Power spectral density of hair-bundle movement. Fitting this spectrum (see Eq. 3 in the Materials and Methods; *red line*) yielded the characteristic frequency $f_0 = 19.8$ Hz; the RMS magnitude $X_{\mathrm{RMS}} = 12.6$ nm; and the quality factor $Q = f_0/\Delta f = 2.3$, where Δf is the width of the spectrum at half the maximal value. (*D*) (*Top*) Negative (*blue*) and positive (*magenta*) position switches were aligned with respect to their switch times (*disks* in *A*) and averaged; the average switch (*thick lines*) is superimposed to the raw segments of oscillation (*thin lines*). (*Bottom*) The speed of the switches was calculated as the time derivative of the mean switches. For clarity, we show here only 40 segments out of a total of ~600 that contributed to the average. Note that positive and negative switches happened at the same speed.

means to increase fluid viscosity and thus viscous drag on the hair bundle. Solutions of high-molecular-weight polymers can form entangled filamentous networks that behave as non-Newtonian porous gels (22). As a result, viscous drag on a moving object can in principle depend on its size, geometry, and shear rate. A viscous solution with large pores relative to the hair-bundle size may only weakly impede hair-bundle movements with respect to viscous drag resulting from standard endolymph. To rule out this possibility, the relation between polymer concentration and viscosity was calibrated by analyzing thermal fluctuations of a flexible fiber's tip (length: ~250 μm; diameter: ~400 nm) and of micron-sized beads (diameter 0.97 and 2.32 μm) in an optical trap (Fig. S2). The different calibration methods yielded identical results. The power spectra of the fluctuations were well described by Lorentzian functions, demonstrating that our solutions had a viscosity that did not depend on the movement frequency and in turn behaved as Newtonian fluids. In addition, viscosity values were close to those measured at a microscopic scale using a viscometer (datasheet from the provider). These calibrations indicated that, for moving objects that are at least 1 μm in size, which is the case for the hair bundle, the sugar solutions behaved as simple fluids with a viscosity that increases exponentially with the sugar concentration. At a concentration of 100 mg/mL, a solution of Dextran 500 had a viscosity ×30 that of regular endolymph. The sugar is a globular molecule with a hydrodynamic radius (4–15 nm) (23) that is comparable to or larger than the size of the conformational change associated to channel gating (14) and too large to go through the transduction channels (24). Although it could increase viscous drag on the micron-sized hair bundle, this viscotropic agent was thus unlikely to affect the kinetics of channel gating and in turn the magnitude of gating friction (9).

We defined the relative viscosity $x = \mu/\mu_0$ of the viscous fluid ($1 < x < 30$), where the viscosity $\mu_0 = 10^{-3}$ kg/(m•s) of standard endolymph, i.e., of endolymph when no polymer was added, is near that of pure water. Because viscous drag is proportional to viscosity, the corresponding friction coefficient $\lambda = x \times \lambda_H$ was proportional to the friction coefficient $\lambda_H = 85$ nN·s·m^{-1} of the hair bundle that was measured in standard endolymph (9).

Model of active hair-bundle motility

We used a physical description of active hair-bundle motility that was previously published (9), but with added noise terms. The simulated positions $\overline{X}$ and $\overline{X}_a$ of hair bundle and adaptation motors, respectively, vary with time according to

$$\lambda \frac{d\overline{X}}{dt} = -K_{GS}\left(\overline{X} - \overline{X}_a - DP_o\right) - K_{SP}\overline{X} + \xi, \qquad (4)$$

$$\lambda_a \frac{d\overline{X}_a}{dt} = K_{GS}\left(\overline{X} - \overline{X}_a - DP_o\right) - F_{\max}(1 - SP_o) + \xi_a. \qquad (5)$$

In addition, we described the finite activation kinetics of the transduction channels by using first-order relaxation kinetics:

$$\tau_C \frac{dP_o}{dt} = P_\infty - P_o + \xi_C. \qquad (6)$$

At thermal equilibrium, the open probability of transduction channels is given by

$$P_\infty = 1/\left\{1 + A\exp\left[-\left(\overline{X} - \overline{X}_a\right)/\delta\right]\right\}, \qquad (7)$$

where $\delta = (k_BT)/(K_{GS}D/N)$, N is the number of transduction elements, and k_BT is the thermal energy. The parameter $A = \exp([\Delta G + (K_{GS}D^2)/(2N)]/(k_BT))$ is related to the intrinsic energy difference $\Delta G = 10\ k_BT$ between open and closed states of the channels. In Eq. 6, the characteristic timescale of transduction channels' activation depends on position according to

$$\tau_C = \tau/\left\{\cosh\left[\left(\overline{X} - \overline{X}_a\right)/(2\delta) - (\ln A)/2\right]\right\}. \qquad (8)$$

There, parameter τ corresponds to the exponential relaxation time of the channels' open probability P_o toward a steady state for which $P_o = P_\infty = 1/2$ in response to a step deflection of the hair bundle from another steady state (9). In Eqs. 4 and 5, λ and λ_a are friction coefficients; K_{GS} and K_{SP} are elastic coefficients; D is the gating swing; and $\xi(t)$, $\xi_a(t)$, and $\xi_C(t)$ are time-dependent, Gaussian noise terms with autocorrelations $\langle\xi(t)\xi(t')\rangle = 2k_BT\ \lambda\ \delta(t - t')$, $\langle\xi_a(t)\xi_a(t')\rangle = 2k_BT_a\ \lambda_a\ \delta(t - t')$, in which $T_a = 1.5T$ is an effective temperature and T is the ambient temperature (10), and $\langle\xi_C(t)\xi_C(t')\rangle = 2\,P_{o,S}\cdot(1 - P_{o,S})\cdot\tau/N\ \delta(t - t')$. In the latter expression, for simplicity, we ignored the dependence of channel-clatter noise on bundle and motor positions and estimated its value at steady state with $P_{o,S} = P_\infty(\overline{X}_S, \overline{X}_{a,S})$ and with a constant channel activation time τ. The gating force Z of a transduction channel, defined as the reduction in gating-spring tension upon channel opening, is given by $Z = K_{GS}D/N$. The deflection $X(t) = \overline{X} - \overline{X}_S$ of the hair bundle and the displacement of the motors $X_a(t) = \overline{X}_a(t) - \overline{X}_{a,S}$ are calculated with respect to their steady-state values $\overline{X}_S$ and $\overline{X}_{a,S}$, respectively.

Stochastic simulations

Simulations and their analysis were performed using MATLAB (version R2015a). Eqs. 4, 5, and 6 were integrated using the Euler method with a step time of 10 μs. The simulated hair-bundle movement $X(t)$ was filtered with an eight-pole Bessel antialiasing filter adjusted to a low-pass half-power frequency of 1 kHz, as in experiments. Using the same procedure as in the analysis of experimental recordings, we then characterized the oscillatory behavior of the system by estimating the channels' open probability $P_{o,S}$, as well as the characteristic frequency f_0, the root-mean-squared magnitude X_{RMS}, the quality factor Q, and the mean switch velocity V_{MAX} of the oscillation.

We generated 50 libraries of 4000 simulations in two cases. Case I: the channels were fast ($\tau = 0$ ms) and friction $\lambda = \lambda_H + \lambda_C$ resulted from the sum of viscous drag λ_H and of an additional source of friction λ_C. We considered 25 values of the friction coefficient λ that were distributed logarithmically within the range 85–5000 nN•s•m^{-1}; the lowest of these values corresponds to viscous drag measured experimentally (9). For each value of λ, we ran 4000 simulations of Eqs. 4, 5, and 6, corresponding to sets of seven parameters that were each randomly chosen within the

TABLE 1 Parameters' Definition and Value for Stochastic Simulations

Parameters	Definition	Value
λ_H	hydrodynamic friction coefficient of the hair bundle	85 nN•s•m^{-1}
λ_C	additional friction coefficient of the hair bundle	0–4915 nN•s•m^{-1}
λ_a	slope of the force-velocity relation of adaptation motors	2–13 μN•s•m^{-1}
K_{GS}	combined stiffness of the gating springs	0.4–0.8 mN•m^{-1}
K_{SP}	combined stiffness of the stereociliary pivots	0.1–0.3 mN•m^{-1}
D	reduction of gating-spring extension upon channel opening	35–63 nm
$F_{\max}$	maximal motor force	43–64 pN
S	calcium feedback strength	0.4–0.8
N	number of transduction elements	40–60
τ	channel activation time near an open probability of 1/2	0.05–5 ms

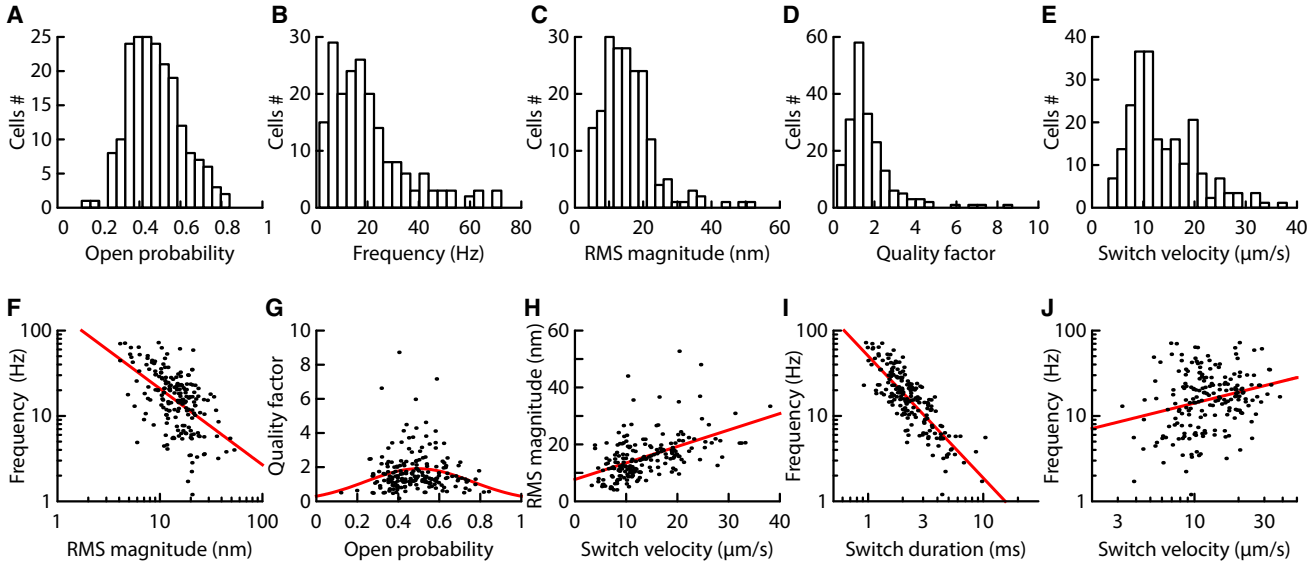

FIGURE 2 Distributions of oscillation characteristics and pairwise relations. Shown here are histograms of the open probability $P_{o,S}$ (*A*), characteristic frequency f_0 (*B*), RMS magnitude X_{RMS} (*C*), quality factor Q (*D*), and switch velocity V_{MAX} (*E*) of hair-bundle oscillations ($n = 196$ cells). Pairwise relations between these characteristics are shown in the following plots. (*F*) The frequency was inversely related to the RMS magnitude (Pearson correlation $r = -0.53$; p value $= 10^{-15}$). A power-law fit to the data yielded $f_0 \propto X_{\mathrm{RMS}}^{-0.89}$ ($R^2 = 0.28$; $[-1.09, -0.69]$, 95% confidence bounds). (*G*) The quality factor is plotted as a function of the open probability. The median value of Q for $0.4 < P_{o,S} < 0.6$ was higher than for the rest of the data points (Mann-Whitney U-test with p value $= 0.003$). (*H*) The RMS magnitude was positively related to the switch velocity (Pearson correlation $r = 0.5$; p value $= 10^{-13}$). The line corresponds to a linear fit $X_{\mathrm{RMS}} = 7.7 + 0.58 \times V_{\mathrm{MAX}}$ ($R^2 = 0.25$). (*I*) The switch duration $\tau_S = 2X_{\mathrm{RMS}}/V_{\mathrm{MAX}}$ was inversely related to the oscillation frequency f_0 (Pearson correlation $r = -0.82$; p value $= 10^{-48}$). The line corresponds to a power-law fit $\tau_S = f_0^{-1.43}$ ($R^2 = 0.67$; $[-1.57, -1.29]$, 95% confidence bounds). (*J*) The frequency f_0 was positively related to the switch velocity V_{MAX} (Pearson correlation $r = 0.26$; p value $= 3 \times 10^{-4}$). A power-law fit to the data yielded $f_0 \propto V_{\mathrm{MAX}}^{0.43}$ ($R^2 = 0.07$; [0.20, 0.65] 95% confidence bounds). To see this figure in color, go online.

intervals given in Table 1. To generate an oscillatory movement $X(t)$ that was compatible with experiments (Fig. 2), we first selected combinations of parameters that satisfied the condition of negative stiffness (i.e., $K_{GS}D/N > 2\sqrt{k_{\mathrm{B}}T(K_{GS} + K_{SP})/N}$). Second, we imposed that the channels' open probability at steady state fell between 0.2 and 0.8 (Fig. 2 *A*). Third, we kept only simulations for which the oscillation frequency was 2–200 Hz (Fig. 2 *B*) and the quality factor was 0.8–15 (Fig. 2 *D*). Finally, we made sure that the simulated position histograms were bimodal (Fig. 1) by imposing that the histogram was well fitted by the sum of two Gaussian functions whose peaks were separated by at least 0.8 times the average half-width of the two peaks.

Case II: the channels had a finite activation time τ and the friction coefficient $\lambda = \lambda_H = 85$ nN•s•m^{-1} resulted from viscous drag only. We considered 25 values of the channel activation time that were logarithmically distributed within the range 0.05–5 ms. For a given value of the channel activation time, we then ran 4000 simulations according to the procedure described in Case I.

For each of the 50 libraries, we determined the best value of the friction coefficient λ (Case I) or of the channel activation time τ (Case II) by maximizing the correlation between the experimental and the simulated distributions of hair-bundle oscillations. We computed 2D histograms for all pairs of oscillation properties among the open probability $P_{o,S}$, the characteristic frequency f_0, the RMS magnitude X_{RMS}, the quality factor Q, and the switch velocity V_{MAX}. From each value of a given property that was obtained in simulations, we subtracted the experimental average and then normalized the result by the experimental SD. For the experimental data, this procedure corresponds to a z-score normalization. Using these normalized variables, the histograms were computed over a fixed grid with a mesh size of 0.1 and smoothed by performing a moving average over a square surface of 7×7 pixels. We quantified the overlap between the experimental and the simulated histograms by calculating their 2D-correlation coefficient (Fig. 5). Because we dealt with five oscillation properties, we obtained 10 correlation coefficients. The net correlation between experimental and simulated distributions of spontaneous oscillations was calculated as the harmonic mean of these 10 coefficients. Note that this procedure takes into account both the distributions of individual oscillation features and their pairwise relations (Fig. 2).

To test the effects of increasing viscosity on simulated hair-bundle oscillations, we selected, within each of our 50 simulation libraries, 14 sets of parameters that best matched the oscillatory properties of the 14 experimentally measured hair bundles for which we had varied endolymph viscosity (Fig. 4). In Case I (fast channels), we assumed that the friction coefficient of the hair bundle could be written as $\lambda = x \times \lambda_H + \lambda_C$, where x was the viscosity relative to that of standard endolymph, while keeping all other parameters unchanged. We ran simulations for 20 values of the normalized viscosity x that were logarithmically distributed between 1 and 30 and characterized the resulting oscillations by estimating the open probability $P_{o,S}$, characteristic frequency f_0, root-mean-squared magnitude X_{RMS}, quality factor Q, and mean switch velocity V_{MAX}. As in experiments, these values were normalized by their corresponding values for $x = 1$ and averaged across the 14 simulated hair bundles. To determine the value of λ_C that best reproduced the experimental data, we calculated the root-mean-squared error between experimental and simulated relations for each oscillation property ($P_{o,S}$, f_0, X_{RMS}, Q, V_{MAX}) as a function of the normalized viscosity x and quantified the deviation between experimental and simulated oscillations by computing the geometrical mean of these five error coefficients. The result is plotted as a function of $\lambda = \lambda_H + \lambda_C$ in Fig. S3 *B*.

In Case II, for which channels had a finite time constant τ and $\lambda_C = 0$, the friction coefficient of the hair bundle was increased proportionally to the normalized viscosity x as $\lambda = x \times \lambda_H$. The procedure was then identical to that used for Case I, except that we here determined the value of the channel activation time τ that best reproduced the experimental data (see Fig. 4, *D–H*, *red lines*). The deviation between simulations and experiments is plotted as a function of τ in Fig. S3 *A*.

RESULTS

Statistics of spontaneous hair-bundle oscillations

We used an excised preparation of the bullfrog's sacculus where hair cells routinely displayed spontaneous oscillations of their hair bundles (see Materials and Methods). We recorded from 196 oscillatory hair bundles to fully characterize the oscillation properties across the population of hair cells (Figs. 1 and 2). As noted before (17,18,25), the hair bundle switched back and forth between two nearly stationary positions (Fig. 1 *A*). Consequently, the probability density of bundle position was bimodal (Fig. 1 *B*). The fractional area under the positive peak yielded an estimate $P_{o,S}$ of the open probability of the transduction channels at steady state (Fig. S1). For the ensemble of cells, the median value of this estimate was $P_{0,S} = 0.47$ (Fig. 2 *A*). Correspondingly, the waveforms of oscillation were approximately rectangular with dwell times at the maximal and minimal positions that were nearly equal. The power-spectral density of bundle movement displayed a clear peak (Fig. 1 *C*) centered at a characteristic frequency f_0 ranging from 2 to 80 Hz (median: 16.4 Hz; Fig. 2 *B*). The root-mean-squared (RMS) magnitude X_{RMS} of oscillation varied between 5 and 50 nm (median: 14.6 nm; Fig. 2 *C*). The degree of regularity of the oscillation could be assessed by computing the ratio of the characteristic frequency and the peak-width of the spectrum at half its maximal height (Fig. 1 *C*). This quantity defined the quality factor Q (range: 0.5–8; median: 1.64; Fig. 2 *D*). The maximal speed V_{MAX} of bundle motion, measured when the bundle switched between its two most-favored positions (Fig. 1 *D*), ranged between 3 and 38 μm/s (median: 11.6 μm/s; Fig. 2 *E*).

Having a large ensemble of oscillatory hair bundles allowed us to probe correlations between pairs of oscillation characteristics. We observed that the characteristic frequency f_0 was inversely correlated with the oscillation magnitude X_{RMS} (Fig. 2 *F*). The largest values of the quality factor occurred near an open probability of $P_{o,S} = 0.5$ (Fig. 2 *G*). Interestingly, the oscillation magnitude X_{RMS} was positively correlated to the switch velocity V_{MAX} (Fig. 2 *H*). A linear fit to the data yielded an offset and a slope. The offset corresponded to the magnitude of position fluctuations that were independent of switching and the slope provided the average duration $\tau_S = 2\Delta X_{\mathrm{RMS}}/\Delta V_{\mathrm{MAX}} = 1.16$ ms of the switch, where the factor 2 resulted from the ratio between the peak-to-peak and root-mean-squared magnitudes of a rectangular waveform. Finally, we also computed the switch duration $\tau_S = 2\,X_{\mathrm{RMS}}/V_{\mathrm{MAX}}$ for individual hair bundles. We found that the oscillation frequency f_0 was inversely correlated to the switch duration τ_S (Fig. 2 *I*). Because the oscillation frequency f_0 decreased more steeply with the switch duration τ_S than with the magnitude X_{RMS}, the oscillation frequency f_0 had to be positively correlated to V_{MAX} (Fig. 2 *J*).

Position switches and negative stiffness

Position switches in the oscillation of a hair bundle have been interpreted as signatures of a mechanical instability by which the bundle traverses a region of negative slope in its force-displacement relation (14). As adaptation strives to set the operating point of the bundle within this unstable region, the bundle periodically jumps across the positions of negative stiffness to reach a stable branch of positive stiffness within its force-displacement relation. Because the mean switch duration τ_S was much shorter (Fig. 2 *H*) than typical adaptation timescales (>10 ms) (26), adaptation motors were expected to remain nearly stationary during a switch. In this case, during the switch, the hair bundle should behave as a simple overdamped system whose dynamics is characterized by force balance between friction and the bundle's elasticity. As a result, the switch velocity is expected to obey $V_{\mathrm{MAX}} \cong \Delta F/\lambda$, where ΔF represents the force difference between the local extrema that flank the negative-stiffness region of the bundle's force-displacement relation and λ is the friction coefficient of the hair bundle. Using a displacement-clamp procedure, we measured the force-displacement relation of 36 oscillatory hair bundles and confirmed that the switch velocity was indeed positively correlated with ΔF (Fig. 3). A linear fit to the data yielded a friction coefficient $\lambda = 430 \pm 80$ nN·s/m (95% confidence bounds). This value is fivefold larger than that of the friction coefficient $\lambda_H \cong 85$ nN·s/m expected from viscous drag on the stereovillar bundle structure, but is remarkably similar to a direct estimate of the bundle's friction coefficient that was obtained by applying periodic force stimuli to the hair bundle (9). Because the friction force that adds to viscous drag can be attributed to gating friction (9), our result suggests that gating friction limits the switch velocity and thus influences the waveform of oscillation.

Oscillations at higher endolymph viscosity

If gating friction is the primary source of passive dissipation in an oscillatory hair bundle, we reasoned that increasing viscous drag, without affecting gating friction, should have minor effects on the oscillation waveform until both friction sources become comparable in magnitude. Adding a polymer of sucrose into endolymph afforded a means to increase fluid viscosity and thus viscous drag on moving objects with the size of the hair bundle (see Materials and Methods and Fig. S2). Upon raising endolymph viscosity, we observed that the frequency of oscillation f_0, as well as the switch velocity V_{MAX}, displayed a nonlinear decrease (Fig. 4). The oscillation frequency remained nearly constant for viscosities up to fourfold that of standard endolymph, decreasing significantly only beyond this value (Fig. 4, *A–D*). The switch velocity also decreased with increasing viscosities (Fig. 4 *E*). This variation was much

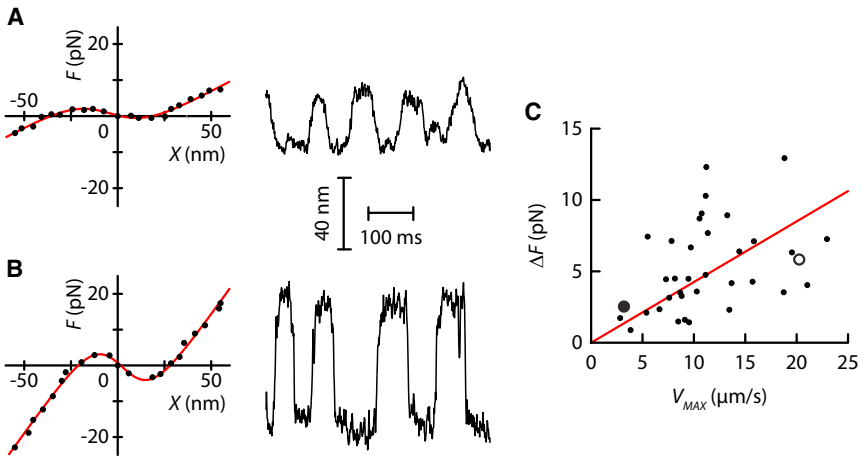

FIGURE 3 Correlation between the force difference ΔF between the local extrema that flank the negative-stiffness region of the bundle's force-displacement relation $F(X)$ and the switch velocity V_{MAX} of a spontaneous hair-bundle oscillation. (*A*) An oscillation with slow switches (*right*; $V_{MAX} = 3.2$ μm/s) displayed a relatively shallow negative-stiffness region in its force-displacement relation (*left*; $\Delta F = 2.5$ pN). (*B*) Another hair bundle produced fast switches (*right*; $V_{MAX} = 20.2$ μm/s), corresponding to a deep negative-stiffness region (*left*; $\Delta F = 5.8$ pN). The lines in (*A*) and (*B*) correspond to fits by Eq. 1 (see Materials and Methods). (*C*) The force difference ΔF was positively correlated to the switch velocity V_{MAX} (Pearson correlation coefficient $r = 0.39$, p value $= 0.02$, $n = 36$). The line represents a linear fit to the data (slope $= 430 \pm 80$ nN·s/m with 95% confidence bounds; $R^2 = 0.03$). The large black and white disks correspond to the hair bundles used for (*A*) and (*B*), respectively. To see this figure in color, go online.

more modest than the inverse-proportionality relation that would be expected if viscous drag limited the velocity of the switch. At a viscosity of ×30, the oscillation frequency and switch velocity had on average decreased by 55% (Fig. 4 *D*) and 66% (Fig. 4 *E*), respectively. Within the same range of viscosities, the oscillation magnitude decreased by only 20% (Fig. 4 *F*). Interestingly, the quality factor of oscillation appeared to slightly increase with viscosity, reaching a maximum at intermediate values (Fig. 4, *B* and *G*). This phenomenon is reminiscent of stochastic resonance (27), a nonlinear phenomenon that may operate in hair cells (28). Finally, the open probability did not vary with endolymph viscosity (Fig. 4 *H*). Overall, hair-bundle oscillations, in particular their characteristic

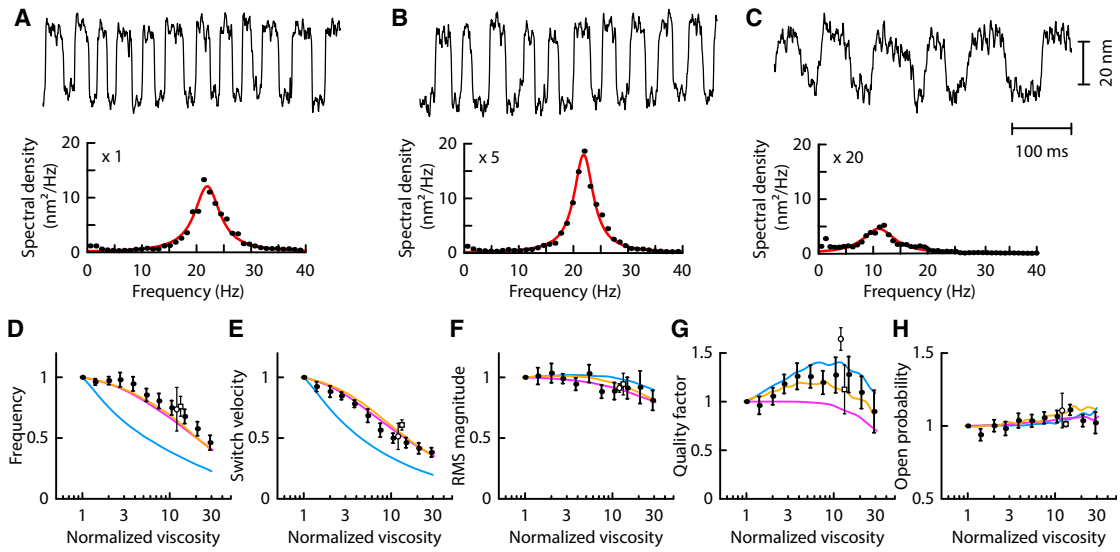

FIGURE 4 Effects of increasing endolymph viscosity on spontaneous hair-bundle oscillations. (*A–C*) Shown here are spontaneous oscillations (*top*) and corresponding power spectra (*bottom*) of a hair bundle that was bathed in endolymph of viscosity ×1 (*A*), ×5 (*B*), and ×20 (*C*) relative to that of standard endolymph. Scale bars apply to all three panels. Characteristic frequency (*D*), switch velocity (*E*), RMS magnitude (*F*), quality factor (*G*), and open probability (*H*) of spontaneous oscillation are given as a function of the normalized viscosity. In (*D–H*), each of the five characteristics of a bundle's oscillation has been normalized by the value measured with standard endolymph and is represented as mean ± SE ($n = 14$ cells). The viscosity was increased by adding various amounts of Dextran 500 to normal endolymph, except for the white square and disk symbols in (*D–H*), where Ficoll 400 and Dextran 40 were used, respectively. (*Blue lines*) Shown here is the simulated behavior when the transduction channels are fast and viscous drag impeding hair-bundle movements is described by the friction coefficient $x \times \lambda_H$, where x is the viscosity relative to that under control conditions (the abscissa of the plot), and $\lambda_H = 85$ nN·s/m is the hydrodynamic drag coefficient of the hair bundle under control conditions. (*Orange lines*) Same but with finite activation kinetics (channel activation time $\tau = 1.1$ ms). (*Magenta lines*) Shown here is the simulated behavior when the transduction channels are fast, and friction on the hair bundle is described by an effective friction coefficient $\lambda = x \times \lambda_H + \lambda_C$ that is the sum of the viscous-drag coefficient $x \times \lambda_H$ and of a constant friction coefficient $\lambda_C = 4.5 \times \lambda_H$ that accounts for an additional source friction. Other parameters are as given in Table 1.

frequencies and switch velocities, appeared relatively insensitive to the imposed variations of endolymph viscosity. These observations make sense if the hair bundle is not only subjected to viscous drag but also to another source of friction that is not significantly affected by the addition of a sugar polymer to endolymph.

Numerical simulations of hair-bundle oscillations

To confirm that gating friction can explain our observations, we used a physical description of active hair-bundle motility (9,29) that can account for both viscous drag and gating friction. In this model, gating friction emerges from the delayed kinetics of the transduction channels (see Materials and Methods). The characteristics of spontaneous oscillations (Fig. 2) and their dependence on viscosity (Fig. 4) were not reproduced by numerical simulations if the transduction channels were fast enough to instantaneously relax to thermal equilibrium, leaving viscous drag as the only friction force on the hair-bundle structure (*blue data points* in Fig. 5 and *blue lines* in Fig. 4). With fast channels, the oscillation frequency and switch velocity ought to decrease steeply with viscosity (Fig. 4, *D* and *E*). In particular, at a viscosity of $\times 4$, the frequency of the simulated oscillations was already half of its initial value whereas experimental oscillations were practically unaffected. In addition, the observed distributions, as well as their pairwise correlations, of the open probability $P_{o,S}$, characteristic frequency f_0, RMS magnitude X_{RMS}, quality factor Q, and switch velocity V_{MAX} of spontaneous oscillations (Fig. 2), could not be matched by simulations with fast channels (Fig. 5 *A*).

Instead, we could explain the experimental data (*orange lines* in Fig. 4, *D–H*; *orange data points* in Fig. 5 *A*) when the activation kinetics of the transduction channels in the model was slow enough that these channels were out of thermal equilibrium. Maximizing the correlation between experimental and simulated distributions of the five oscillation characteristics ($P_{o,S}$, f_0, X_{RMS}, Q, and V_{MAX}) by varying the channel activation time τ in the model provided the estimate $\tau = 0.8 \pm 0.4$ ms (half-width at 90% maximum; Fig. 5 *B*). A global fit to the dependence of these five characteristics on viscosity (*orange line* in Fig. 4, *D–H*; Fig. S3 *A*) provided a similar value $\tau = 0.4$–2 ms, although there was not a clear optimum within this range. The two estimates of the channel activation time are compatible with a previous assessment on single oscillatory hair bundles (9). However, the transduction channels appear here to be significantly slower than in early measurements of trans-epithelial currents from the entire bullfrog's sacculus (11).

Finally, we also considered an effective description of hair-bundle mechanics where the transduction channels instantaneously relax to their open probability at thermal equilibrium. Gating friction was captured by a contribution λ_C to the friction coefficient $\lambda = \lambda_H + \lambda_C$ of the hair bundle (see Materials and Methods) (10). This effective description also provided a good fit to the experimental data (*magenta line* in Fig. 4, *D–H*; Fig. S3 *B*; *magenta data points* in Fig. 5). We noted, however, that the dependence of the quality factor on the normalized viscosity was better described when the finite activation kinetics of the channels was taken into account (Fig. 4 *G*; compare *orange* and *magenta lines*). Maximizing the correlation between experimental and simulated distributions of the five oscillation characteristics (Fig. 5 *C*) or a global fit of the dependence of these characteristics on viscosity (Fig. S3 *B*) yielded a value $\lambda_C = (3-8) \times \lambda_H$. This value agrees with direct estimates of gating friction through dynamic force measurements (9). Comparing the model that includes channel kinetics and the effective model confirms that the transduction channels produce internal friction forces corresponding to a friction coefficient almost one order-of-magnitude larger than that associated with viscous drag on the hair bundle.

Varying the activation time of the transduction channels affords a means to modulate the magnitude of gating friction (9). Although experimentally impractical, this task could readily be performed in simulations (Fig. 6). The overall relation between the channel activation time and the oscillation frequency displayed low-pass characteristics: the frequency plateaued at a maximal value for $\tau < 100$ μs and showed a logarithmic decline for $\tau > 1$ ms. With a channel activation time $\tau = 1$ ms, a value that accords with our experiments (Fig. 5 *B*; Fig. S3 *A*), we observed that the oscillation frequency was 25% lower than with fast channels ($\tau = 0$). Our simulations thus indicate that the characteristic frequency of observed hair-bundle oscillations is set in part by the finite activation kinetics of the transduction channels.

DISCUSSION

Gating friction shapes hair-bundle oscillations

Our detailed analysis of spontaneous hair-bundle oscillations and their dependence on endolymph viscosity betrays several signatures of friction from transduction channels' gating. First, the maximal speed of the position switches within the rectangular waveform of oscillation is too low to be limited by viscous drag only, indicating that an additional friction impedes these movements (Fig. 3 and *blue points* in Fig. 5). Positive and negative switches of bundle position are associated, respectively, with opening and closing of the transduction channels (16,17,21). It is precisely during gating that friction on the hair bundle is expected to increase (9,15). Second, the switch velocity and the oscillation frequency are only marginally affected by an increase of endolymph viscosity by up to 30-fold (Fig. 4). This result is consistent with the existence of an intrinsic source of friction that dominates viscous drag and whose magnitude does not vary significantly with

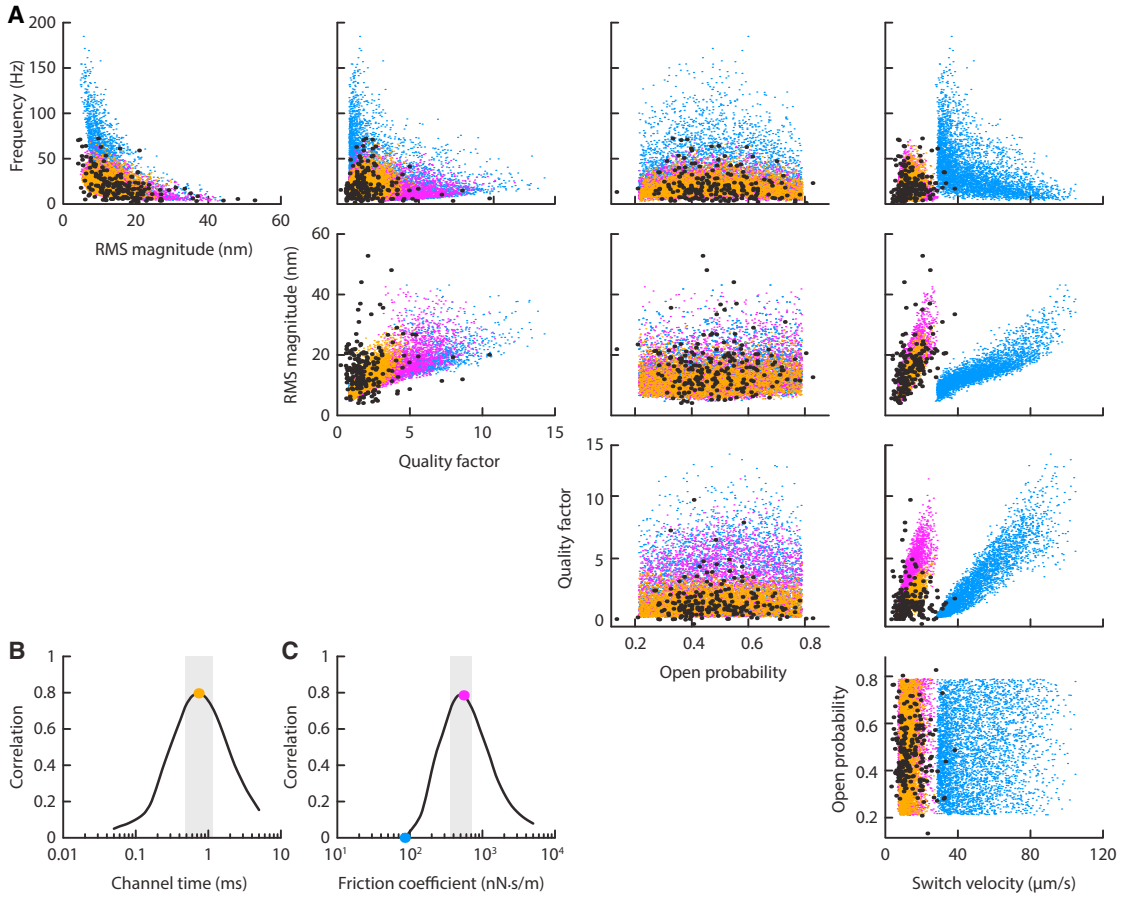

FIGURE 5 Comparing the characteristics of simulated and experimental hair-bundle oscillations. (*A*) We plot here pairwise relations between the distributions of oscillation properties for experimental (*black*) and simulated (*blue*, *orange*, and *magenta*) data. (*Blue*) These data points result from simulations of 4000 oscillatory hair bundles with fast channels (channel activation time $\tau = 0$ ms) and friction coefficient $\lambda = \lambda_H = 85$ nN·s·m^{-1}, corresponding to the measured value of viscous drag on the hair bundle in standard endolymph. Other parameters were $\lambda_a = 9.1 \pm 3.6$ μN·s·m^{-1}, $K_{GS} = 0.65 \pm 0.09$ mN·m^{-1}, $K_{SP} = 0.19 \pm 0.06$ mN·m^{-1}, $D = 50.9 \pm 3.5$ nm, $F_{max} = 57 \pm 4$ pN, and $S = 0.66 \pm 0.11$. (*Orange*) In these simulations, channels had finite activation kinetics ($\tau = 0.7$ ms) and $\lambda = \lambda_H = 85$ nN·s·m^{-1}. At this value of τ, the correlation between experimental and simulated distributions of hair-bundle oscillations was maximal (*orange disk* in *B*). Other parameters were $\lambda_a = 8.8 \pm 3.7$ pN·s/nm, $K_{GS} = 0.64 \pm 0.09$ pN/nm, $K_{SP} = 0.19 \pm 0.06$ pN/nm, $D = 50.5 \pm 3.5$ nm, $F_{max} = 57 \pm 4$ pN, and $S = 0.60 \pm 0.11$. (*Magenta*) As in blue, but with an increased friction coefficient $\lambda = 550$ nN·s·m$^{-1} \cong 6 \times \lambda_H$. At this value of λ, the correlation between the experimental and the simulated distributions of hair-bundle oscillations was maximal (*magenta disk* in *C*). (*B*) Given here is the correlation coefficient between experimental and simulated distributions of oscillation properties as a function of the channel activation time τ, assuming that the hair bundle was subjected to viscous drag only, i.e., $\lambda = \lambda_H = 85$ nN·s·m^{-1}. The relation peaked within a range $\tau = 0.5$–1.3 ms (*shaded area*; width at 90% maximum). (*C*) The correlation coefficient between experimental and simulated distributions of oscillation properties is plotted as a function of the friction coefficient λ, assuming that the transduction channels were fast, i.e., $\tau = 0$ ms. The relation peaked within a range $\lambda = 350$–800 nN·s·m^{-1} (*shaded area*; width at 90% maximum), corresponding to friction coefficients that were 4–9-fold larger than that provided by viscous drag ($\lambda_H = 85$ nN·s·m^{-1}). Accordingly, the hair bundle was effectively subjected to an additional source of friction $\lambda_C = \lambda - \lambda_H = 265$–$715$ nN·s·m^{-1}, which was 3–8-fold larger than λ_H.

the addition of a polymer of sucrose in endolymph. Accordingly, this viscotropic agent increases viscous drag on micron-sized objects like the hair bundle but is unlikely to affect the kinetics of channel gating and in turn the magnitude of gating friction (see Materials and Methods). Third, the pairwise correlations of oscillation characteristics are reproduced by our description of hair-bundle mechanics when the finite activation kinetics of the transduction channels is included (Fig. 5). An effective description with fast channels but for which a constant (λ_C) is added to the hydrodynamic friction coefficient (λ_H) of the hair bundle also accounts for the data. Together, these two observations confirm that the finite activation kinetics of the channels results in an additional source of hair-bundle friction (9,15). They also qualify the effective description as a simplified model to account for gating friction (10).

Gating friction is related to channel kinetics

The gating friction coefficient λ_C in the effective model can be related to the activation time τ of a transduction channel in the full model. For a channels' open probability $P_{o,S}$ near 1/2, the gating friction coefficient can be

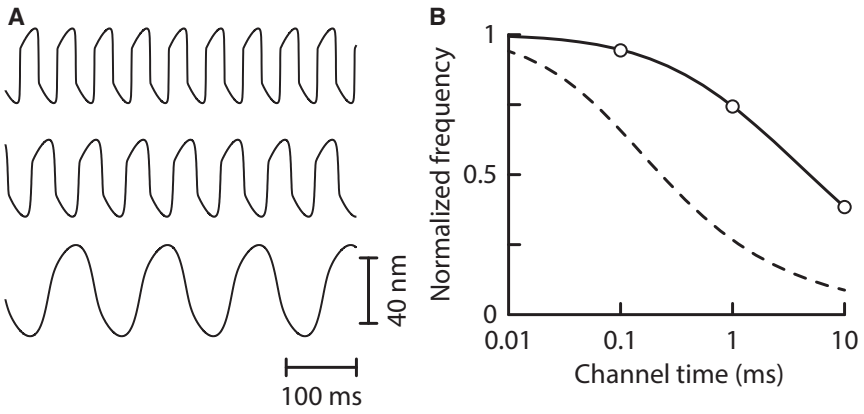

FIGURE 6 Simulated hair-bundle oscillations as a function of the channels' activation time. (*A*) Shown here are simulations of hair-bundle oscillations with a channel activation time of 0.1, 1, and 10 ms, from top to bottom, respectively. (*B*) The normalized oscillation frequency is plotted as a function of the channel's activation time τ (*solid line*) with parameter values $N = 50$, $K_{GS} = 0.6$ pN/nm, $K_{SP} = 0.3$ pN/nm, $D = 60$ nm, $\lambda_H = 85$ nN·s·m^{-1}, $\lambda_a = 10$ μN·s·m^{-1}, $S = 0.7$, and $F_{max} = 53$ pN. The three disks correspond to data shown in (*A*). The dotted line corresponds to the expected variation $1/\sqrt{1+\tau/\tau_R}$ when the hair bundle operates precisely the Hopf bifurcation, where $\tau_R \cong \lambda_H/K_\infty$ is the mechanical relaxation time of the hair bundle.

approximated as $\lambda_C \cong \Delta K \times \tau$ (9,10,15). The prefactor $\Delta K = [NZ^2/(4\ k_BT)]$ has units of stiffness and corresponds to the maximal gating compliance produced by N transduction channels that operate in parallel in the hair bundle. Here, Z is the internal force produced by gating of a transduction channel—the gating force—where k_B is the Boltzmann constant and T is temperature. Thus, the slower the channels, the higher the friction that is produced by channel gating. Comparing the friction coefficient associated with gating friction (λ_C) to that resulting from viscous drag (λ_H), we find that gating friction dominates viscous drag if the transduction channels are slower than a characteristic time $\tau_Ø = 4\ k_BT\ \lambda_H/(NZ^2)$. With typical values, $N = 50$, $Z = 0.75$ pN, and $\lambda_H = 85$ nN·s·m^{-1}, we find $\tau_Ø = 50$ μs. This value is one order-of-magnitude lower than the channel activation time estimated here to account for the characteristics of spontaneous oscillations (Fig. 5 *B*). This explains why experimental estimates of λ_C (Fig. 5 *C*; Fig. S3 *B*) are up to one order-of-magnitude larger than the friction coefficient λ_H associated to viscous drag.

We note that our estimate $\tau \approx 1$ ms for the channel activation time (Fig. 5 *B*; Fig. S3 *A*) is significantly larger than an estimate that was published previously (11). In this seminal work, the exponential activation kinetics of transduction currents evoked by step deflections of the hair bundles yielded time constants that varied from 100 to 500 μs at 4°C, with larger stimuli resulting in shorter activation times. After correction for the dependence of channel kinetics on temperature, one would expect the channel activation time to be no longer than 125 μs at 23°C. If the transduction channels were this fast, gating friction would be approximately one order-of-magnitude smaller than estimated here and measured previously (9). Thus, our results imply that the channels are slower in our experiments. This difference may arise because channel kinetics was previously measured from an average response over hundreds of hair cells that were stimulated simultaneously to produce a trans-epithelial current, whereas we studied single hair bundles. In addition, we only worked with hair bundles that oscillated spontaneously.

The oscillation frequency depends on the channel activation time

Spontaneous oscillations of the hair bundle have a period f_0^{-1} (~100 ms) that is two orders-of-magnitude larger than the activation time τ of the channels (~1 ms). Yet, the channels are slow enough to affect the characteristic frequency of oscillation (Fig. 6). Why does channel kinetics slow down the oscillations? Our theoretical description of active hair-bundle motility (see Materials and Methods) provides a simple framework to discuss the physical parameters that control the oscillation frequency. Spontaneous oscillations emerge from an interplay between negative hair-bundle stiffness, adaptation motors, and feedback by the calcium component of the transduction current (16,17). An oscillatory instability called a "Hopf bifurcation" occurs when this active dynamical system cancels both friction forces and elastic restoring forces (6,30–32).

Precisely at the Hopf bifurcation, the characteristic frequency of spontaneous oscillation depends on channel activation time as $f_C(\tau) = f_C(0)/\sqrt{1+\tau/\tau_R}$, where $f_C(0)$ is the oscillation frequency when the channels are fast and $\tau_R \cong \lambda_H/K_\infty$ is the mechanical relaxation time of the hair bundle, given its hydrodynamic friction coefficient λ_H and its stiffness K_∞ at large deflections (see the Supporting Material). Thus, at the Hopf bifurcation, the channel activation time τ must be compared to the bundle's mechanical relaxation time τ_R to determine whether channel kinetics has a significant effect on the frequency of the oscillation. With $K_\infty = 0.9$ mN·m^{-1} and $\lambda_H = 85$ nN·s·m^{-1} (Table 1), we get $\tau_R \cong 100$ μs. The mechanical relaxation time is thus one order-of-magnitude smaller than our estimate $\tau \cong 1$ ms of the channel activation time. With $\tau/\tau_R \cong 10$, the frequency of spontaneous oscillation is expected to be only one-third that predicted with fast channels (Fig. 6 *B*; *dashed line*).

Away from the Hopf bifurcation, there is no analytic expression of the oscillation frequency. With parameter values that accord with the oscillations observed in our experiments, simulations nevertheless indicate that the effect of slow channel kinetics is less dramatic than at the Hopf bifurcation but nevertheless significant (Fig. 6 *B*; *solid line*). We observe that the simulated dependences of the oscillation frequency on endolymph viscosity and on the channel activation time have a similar shape (compare *orange line* in Fig. 4 *D* and *black solid line* in Fig. 6 *B*). This similarity arises because in both cases the effective friction $\lambda = \lambda_H + \lambda_C$ increases linearly along the abscissa. Indeed, in one case λ_H varies in proportion to endolymph viscosity with λ_C constant (Fig. 4 *D*), whereas in the other case λ_C varies in proportion to the channel activation time with λ_H constant (Fig. 6 *B*). The fact that this simple argument works confirms that the effect of channel kinetics on hair-bundle mechanics can be captured by introducing an effective friction coefficient.

In conclusion, our work shows that the activation kinetics of the transduction channels and the friction forces produced by delayed channel gating play a key role in shaping spontaneous oscillations of mechanosensory hair bundles. Spontaneous oscillations power frequency-selective amplification of weak mechanical stimuli. Thus, we demonstrate a direct role of the transduction channels' gating properties in this active process. In particular, the oscillation frequency is set in part by the channel activation time. Mechanosensitivity of vertebrate hair bundles is mediated by a common architecture comprising transduction channels mechanically coupled to tip links. As a result, hair bundles share a fundamental physical property: they are subjected to forces associated with gating of the transduction channels. Gating compliance and gating friction are thus inherent mechanical features to hair bundles. In the case of oscillatory hair bundles, varying the channel activation time (33,34) provides a fundamental mechanism to mechanically tune the characteristic frequency of hair cells along the tonotopic axis of auditory organs.

SUPPORTING MATERIAL

Supporting Materials and Methods and three figures are available at http://www.biophysj.org/biophysj/supplemental/S0006-3495(17)31251-1.

AUTHOR CONTRIBUTIONS

J.B., F.J., and P.M. designed research, performed research, analyzed data, and wrote the manuscript.

ACKNOWLEDGMENTS

We thank Benjamin Lindner, Kai Dierkes, and Volker Bormuth for stimulating discussions.

This research was supported by the French National Agency for Research (ANR-11-BSV5 0011), Labex Celtisphybio ANR-10-LABX-0038 part of the Idex PSL, and by the National Science Foundation under grant NSF PHY11-25915. J.B. was supported by a Human Frontier Science Program long-term postdoctoral fellowship (LT000132/2012) and by the Bettencourt Schueller Foundation.

REFERENCES

1. Hudspeth, A. J. 1989. How the ear's works work. *Nature*. 341:397–404.
2. Martin, P. 2008. Active hair-bundle motility of the hair cells of vestibular and auditory organs. *In* Active Processes and Otoacoustic Emissions. G. A. Manley, A. N. Popper, and R. R. Fay, eds. Springer, New York, New York, pp. 93–144.
3. Barral, J., and P. Martin. 2011. The physical basis of active mechanosensitivity by the hair-cell bundle. *Curr. Opin. Otolaryngol. Head Neck Surg*. 19:369–375.
4. Martin, P., and A. J. Hudspeth. 1999. Active hair-bundle movements can amplify a hair cell's response to oscillatory mechanical stimuli. *Proc. Natl. Acad. Sci. USA*. 96:14306–14311.
5. Hudspeth, A. J. 2008. Making an effort to listen: mechanical amplification in the ear. *Neuron*. 59:530–545.
6. Hudspeth, A. J., F. Jülicher, and P. Martin. 2010. A critique of the critical cochlea: Hopf—a bifurcation—is better than none. *J. Neurophysiol*. 104:1219–1229.
7. Crawford, A. C., and R. Fettiplace. 1985. The mechanical properties of ciliary bundles of turtle cochlear hair cells. *J. Physiol*. 364:359–379.
8. Kozlov, A. S., J. Baumgart, …, A. J. Hudspeth. 2011. Forces between clustered stereocilia minimize friction in the ear on a subnanometre scale. *Nature*. 474:376–379.
9. Bormuth, V., J. Barral, …, P. Martin. 2014. Transduction channels' gating can control friction on vibrating hair-cell bundles in the ear. *Proc. Natl. Acad. Sci. USA*. 111:7185–7190.
10. Nadrowski, B., P. Martin, and F. Jülicher. 2004. Active hair-bundle motility harnesses noise to operate near an optimum of mechanosensitivity. *Proc. Natl. Acad. Sci. USA*. 101:12195–12200.
11. Corey, D. P., and A. J. Hudspeth. 1983. Kinetics of the receptor current in bullfrog saccular hair cells. *J. Neurosci*. 3:962–976.
12. Markin, V. S., and A. J. Hudspeth. 1995. Gating-spring models of mechanoelectrical transduction by hair cells of the internal ear. *Annu. Rev. Biophys. Biomol. Struct*. 24:59–83.
13. Howard, J., and A. J. Hudspeth. 1988. Compliance of the hair bundle associated with gating of mechanoelectrical transduction channels in the bullfrog's saccular hair cell. *Neuron*. 1:189–199.
14. Martin, P., A. D. Mehta, and A. J. Hudspeth. 2000. Negative hair-bundle stiffness betrays a mechanism for mechanical amplification by the hair cell. *Proc. Natl. Acad. Sci. USA*. 97:12026–12031.
15. Bormuth, V., J. Barral, …, P. Martin. 2015. Hair-bundle friction from transduction channels' gating forces. *AIP Conf. Proc*. 1703:030003.
16. Tinevez, J. Y., F. Jülicher, and P. Martin. 2007. Unifying the various incarnations of active hair-bundle motility by the vertebrate hair cell. *Biophys. J*. 93:4053–4067.
17. Martin, P., D. Bozovic, …, A. J. Hudspeth. 2003. Spontaneous oscillation by hair bundles of the bullfrog's sacculus. *J. Neurosci*. 23:4533–4548.
18. Martin, P., A. J. Hudspeth, and F. Jülicher. 2001. Comparison of a hair bundle's spontaneous oscillations with its response to mechanical stimulation reveals the underlying active process. *Proc. Natl. Acad. Sci. USA*. 98:14380–14385.
19. Jülicher, F., K. Dierkes, …, P. Martin. 2009. Spontaneous movements and linear response of a noisy oscillator. *Eur. Phys. J. E Soft Matter*. 29:449–460.
20. Ramunno-Johnson, D., C. E. Strimbu, …, D. Bozovic. 2009. Distribution of frequencies of spontaneous oscillations in hair cells of the bullfrog sacculus. *Biophys. J*. 96:1159–1168.

21. Meenderink, S. W., P. M. Quiñones, and D. Bozovic. 2015. Voltage-mediated control of spontaneous bundle oscillations in saccular hair cells. *J. Neurosci.* 35:14457–14466.

22. Hunt, A. J., F. Gittes, and J. Howard. 1994. The force exerted by a single kinesin molecule against a viscous load. *Biophys. J.* 67:766–781.

23. Armstrong, J. K., R. B. Wenby, …, T. C. Fisher. 2004. The hydrodynamic radii of macromolecules and their effect on red blood cell aggregation. *Biophys. J.* 87:4259–4270.

24. Farris, H. E., C. L. LeBlanc, …, A. J. Ricci. 2004. Probing the pore of the auditory hair cell mechanotransducer channel in turtle. *J. Physiol.* 558:769–792.

25. Clausznitzer, D., B. Lindner, …, P. Martin. 2008. Two-state approach to stochastic hair bundle dynamics. *Phys. Rev. E Stat. Nonlin. Soft Matter Phys.* 77:041901.

26. Hacohen, N., J. A. Assad, …, D. P. Corey. 1989. Regulation of tension on hair-cell transduction channels: displacement and calcium dependence. *J. Neurosci.* 9:3988–3997.

27. Gammaitoni, L., P. Hänggi, …, F. Marchesoni. 1998. Stochastic resonance. *Rev. Mod. Phys.* 70:223–287.

28. Indresano, A. A., J. E. Frank, …, F. Jaramillo. 2003. Mechanical noise enhances signal transmission in the bullfrog sacculus. *J. Assoc. Res. Otolaryngol.* 4:363–370.

29. Han, L., and A. B. Neiman. 2010. Spontaneous oscillations, signal amplification, and synchronization in a model of active hair bundle mechanics. *Phys. Rev. E Stat. Nonlin. Soft Matter Phys.* 81:041913.

30. Camalet, S., T. Duke, …, J. Prost. 2000. Auditory sensitivity provided by self-tuned critical oscillations of hair cells. *Proc. Natl. Acad. Sci. USA.* 97:3183–3188.

31. Eguíluz, V. M., M. Ospeck, …, M. O. Magnasco. 2000. Essential nonlinearities in hearing. *Phys. Rev. Lett.* 84:5232–5235.

32. Choe, Y., M. O. Magnasco, and A. J. Hudspeth. 1998. A model for amplification of hair-bundle motion by cyclical binding of Ca^{2+} to mechanoelectrical-transduction channels. *Proc. Natl. Acad. Sci. USA.* 95:15321–15326.

33. Ricci, A. 2002. Differences in mechano-transducer channel kinetics underlie tonotopic distribution of fast adaptation in auditory hair cells. *J. Neurophysiol.* 87:1738–1748.

34. Ricci, A. J., H. J. Kennedy, …, R. Fettiplace. 2005. The transduction channel filter in auditory hair cells. *J. Neurosci.* 25:7831–7839.

Biophysical Journal, Volume *114*

Supplemental Information

Friction from Transduction Channels' Gating Affects Spontaneous Hair-Bundle Oscillations

Jérémie Barral, Frank Jülicher, and Pascal Martin

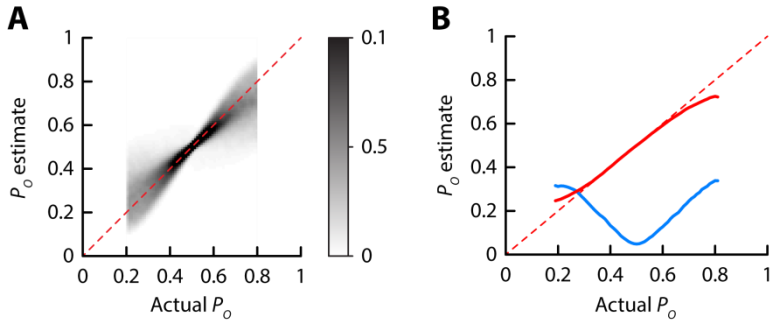

Figure S1: Using simulations to compare an estimate of the transduction channels' open probability at steady state (noted $P_{o,S}$ in the main text) to its actual value.

(A) For each simulated oscillation, we fitted the bimodal distribution of positions by the sum of two Gaussian functions. The estimate of the transduction channels' open probability at steady state, which is noted $P_{o,S}$ in the main text, is defined as the fractional area under the Gaussian that was centered at a positive position with respect to the mean bundle position. We used our 50 libraries of simulated oscillations (see Methods) to compare this estimate to the actual value of the steady-state open probability over a wide range of parameter values. We plot here a two-dimensional histogram of the data using a bin size of 0.01 for both the abscissa and the ordinate. The red dashed line has a slope of unity. Note that no open probabilities are found below $P_o = 0.2$ or above $P_o = 0.8$ because this criterion was used for defining an oscillatory hair bundle (see Methods). **(B)** Using the data shown in **(A)**, for each value of the actual P_o, we then calculated the mean value of the P_o estimate and the full width at half the maximal height of the histogram; they are plotted here as a function of the actual P_o (red and blue lines, respectively).

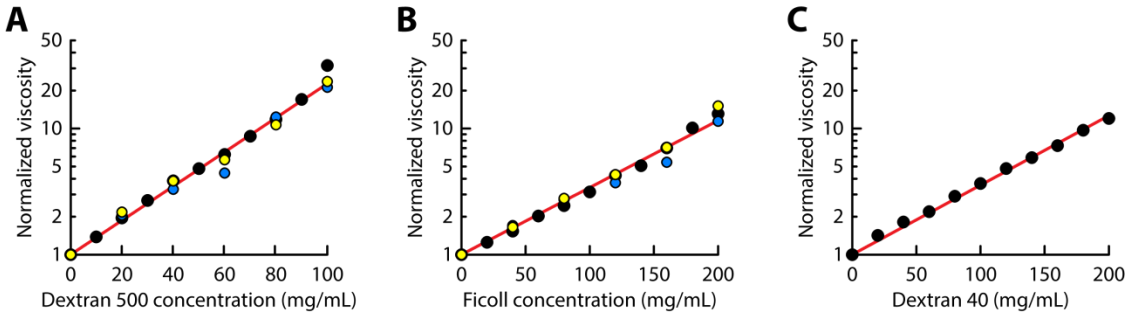

Figure S2: Increasing endolymph viscosity by adding a polymer of sucrose.

The relation between polymer concentration (**(A)**: Dextran 500; **(B)**: Ficoll PM 400; **(C)**: Dextran 40) and viscosity was calibrated by measuring the friction coefficient λ of a flexible fiber (black) or of micro-beads of diameter 0.97 μm (blue) or 2.32 μm (yellow) immersed in the solution. The friction coefficient of a flexible fiber or of a bead maintained in an optical trap was evaluated by measuring their Brownian fluctuations. The power spectrum of spontaneous movement was adjusted by a Lorentzian function $S(\omega) = \frac{2k_B T \lambda_F}{{k_F}^2 + (\omega \lambda_F)^2}$ from which the friction (λ_F) and stiffness (k_F) coefficients were extracted. For viscous drag, the relative increase in friction is equal to the relative increase in viscosity: $\mu/\mu_0 = \lambda/\lambda_0 = x$, where μ is the viscosity of endolymph in which the friction coefficient of the object is λ and the subscript '0' denotes the endolymph of reference with no-added polymer. The relation between the normalized viscosity x and the sugar concentration was fitted by an exponential function (red lines).

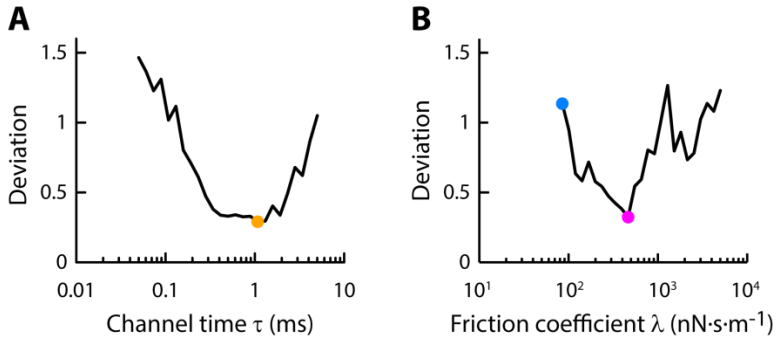

Figure S3: Deviation between experiments and simulations when studying the effects of endolymph viscosity on hair-bundle oscillations.

(A) The channels are slow ($\tau > 0$) and the bundle's friction coefficient is given by $\lambda = x \times \lambda_H$, where $1< x <30$ is the normalized viscosity of endolymph and λ_H corresponds to viscous drag in standard endolymph, i.e. for $x = 1$. For each of the five oscillation properties ($P_{o,S}$, f_0, X_{RMS}, Q, V_{MAX}), we computed the root-mean-squared error between experimental and simulated relations between the oscillation property and the normalized endolymph viscosity $1< x <30$. The deviation between experiments and simulations was defined as the geometrical mean of the 5 error coefficients and is here plotted as a function of the channel activation time τ. The orange disk marks the value of τ for which the deviation is minimal, corresponding to the orange lines in Fig. 4 of the main text. **(B)** The channels are fast ($\tau = 0$) and the hair bundle is subjected to an effective friction coefficient $\lambda = \lambda_H + \lambda_C$. The blue and magenta disks mark, respectively, the value of λ for which there is no channel friction ($\lambda = \lambda_H$; $\lambda_C = 0$) and the value of λ that minimizes the deviation between simulations and experimental data. They correspond to the blue and magenta lines in Fig. 4, respectively. The deviation was computed as in **(A)**.

SUPPORTING TEXT

Stability analysis of the hair-bundle model: oscillation frequency at the Hopf bifurcation.

We consider the model of active hair-bundle motility given by equations 4-8 of the main text (Methods section). We omit noise terms on the right-hand side of equations 4-6 and assume an open probability $P_{o,S} = 1/2$ at steady state, which approximates the median value observed in experiments (Fig. 2C). By performing a linear-stability analysis of this system of coupled differential equations, we aim at determining an analytical expression for the frequency of spontaneous oscillation at a Hopf bifurcation. Taking small deviations $X = \bar{X} - \bar{X}_S$, $X_a = \bar{X}_a - \bar{X}_{a,S}$, and $\delta P_o = P_o - P_{o,S}$, respectively, of the position $\bar{X}$ of the hair bundle, of the position $\bar{X}_a$ of the adaptation motors, and of the open probability P_o of the transduction channels with respect to their values at steady state, we can linearize the system and write:

$$\begin{pmatrix} \dot{X} \\ \dot{X}_a \\ \delta\dot{P}_o \end{pmatrix} = \boldsymbol{J} \begin{pmatrix} X \\ X_a \\ \delta P_o \end{pmatrix}, \tag{S1}$$

where the Jacobian matrix $\boldsymbol{J}$ is given by:

$$\boldsymbol{J} = \begin{pmatrix} -(K_{GS} + K_{SP})/\lambda_H & K_{GS}/\lambda_H & K_{GS}D/\lambda_H \\ K_{GS}/\lambda_a & -K_{GS}/\lambda_a & -K_{GS}D\left(1 - \frac{SF_{max}}{K_{GS}D}\right)/\lambda_a \\ P'_\infty/\tau & -P'_\infty/\tau & 1/\tau \end{pmatrix}, \tag{S2}$$

The parameters are defined in the Methods section and in Table 1 of the main text. Dots and primes in superscript denote time and spatial derivatives, respectively. Note that with $P_{o,S} = 1/2$, the channel activation time $\tau_C(X) \cong \tau$ does not depend on the bundle position X at the linear order. The eigenvalues s of the Jacobian obey:

$$\det|\boldsymbol{J} - s\mathbf{1}| = 0, \tag{S3}$$

in which $\mathbf{1}$ denotes the identity matrix. We must then find the roots of a third-order polynomial:

$$s^3 + s^2\left(\frac{1}{\tau} + \frac{K_{GS}}{\lambda_a} + \frac{K_\infty}{\lambda_H}\right) + s\left(\frac{\tilde{K}_{GS}}{\lambda_a\tau} + \frac{K_{HB}}{\lambda_H\,\tau} + \frac{K_{SP}K_{GS}}{\lambda_a\,\lambda_H}\right) + \frac{K_{SP}\tilde{K}_{GS}}{\lambda_a\,\lambda_H\,\tau} = 0\,, \tag{S4}$$

in which we have introduced the combined stiffness $K_\infty = K_{GS} + K_{SP}$ of the stereociliary pivots and of the gating springs, the stiffness $\widetilde{K}_{GS} = K_{GS}\left[1 - D\left(1 - \frac{SF_{max}}{K_{GS}D}\right) P'_\infty\right]$ of the effective gating spring that exerts an elastic restoring force on the adaptation motors, and the stiffness $K_{HB} = K_{GS}(1 - D\,P'_\infty) + K_{SP}$ of the hair bundle with gating compliance. Note that the stiffness $\widetilde{K}_{GS}$ depends both on gating compliance and on calcium feedback.

At a Hopf bifurcation, there is a pair of complex-conjugate eigenvalues that are purely imaginary. We can thus write $s = \pm i\omega_c$, where $i^2 = -1$ and $\omega_c = 2\pi\, f_C$ represents the angular frequency of spontaneous oscillation. Injecting this Ansatz into Eq. S4 and taking the real part of the resulting equation, we find:

$$\omega_c = \omega_c(\tau = 0)/\sqrt{1 + \tau/\tau_R}\,, \tag{S5}$$

There, the angular frequency

$$\omega_c(\tau = 0) = \sqrt{\frac{K_{SP}}{\lambda_H} \times \frac{\widetilde{K}_{GS}}{\lambda_a}} = 1/\sqrt{\tau_{SP} \times \tau_a} \tag{S6}$$

represents the oscillation frequency when the channels are infinitely fast ($\tau = 0$). In this equation, we recognize the passive relaxation times $\tau_{SP} = \lambda_H/K_{SP}$ of the hair-bundle position to small force steps when the bundle's stiffness is reduced to the contribution K_{SP} of the stereociliary pivots and the timescale $\tau_a = \lambda_a/\widetilde{K}_{GS}$ of adaptation in response to small step displacements of the hair bundle (1). Channel kinetics affects the oscillation frequency when the channel activation time τ becomes large enough to be comparable to or larger than a characteristic timescale τ_R with

$$\tau_R = 1/\left(\frac{K_{GS}}{\lambda_a} + \frac{K_\infty}{\lambda_H}\right) \tag{S7}$$

With typical parameter values (Table 1), $\lambda_a/K_{GS} \cong 100 \times \lambda_H/K_\infty$. Thus, $\tau_R \cong \lambda_H/K_\infty$. This is the passive relaxation time of the hair bundle in response to small force steps at timescales short enough that the channels have no time to gate and produce gating compliance.

SUPPORTING REFERENCES

1. Tinevez, J. Y., F. Jülicher, and P. Martin. 2007. Unifying the various incarnations of active hair-bundle motility by the vertebrate hair cell. Biophys. J. 93:4053-4067.